Journal of Catalysis **209,** 202–209 (2002)
doi:10.1006/jcat.2002.3617

Nickel–Magnesia Catalysts: An Alternative for the Hydrogenation of 1,6-Hexanedinitrile

Marc Serra,* Pilar Salagre,*,[1] Yolanda Cesteros,* Francisco Medina,† and Jesús E. Sueiras†

*Facultat de Química, Universitat Rovira i Virgili, 1.43005, Tarragona, Spain; and †Escola Tècnica Superior d'Enginyeria Química, Universitat Rovira i Virgili, Av. Països Catalans, 26, 43007, Tarragona, Spain

Received January 8, 2002; revised March 21, 2002; accepted March 21, 2002

Two Ni–MgO systems were synthesized and characterized as nickel catalysts for the hydrogenation of 1,6-hexanedinitrile (adiponitrile) in the gas phase. The activity results were compared with those obtained for a commercial Raney–Ni. All three catalysts showed high selectivity to 1,6-hexanediamine, for a total conversion with a maximum of 96% for the Ni–MgO catalyst, which was made from a NiO–MgO solution. However, only Ni–MgO catalysts showed high selectivity to 6-aminohexanenitrile (83 and 77%, respectively) and high conversion (87 and 85%, respectively). The higher selectivity to 6-aminohexanenitrile could be related to the presence of octahedral crystallites in the Ni–MgO catalysts.

Key Words: **nickel–magnesia catalysts; magnesia; adiponitrile; dinitrile; 1,6-hexanedinitrile hydrogenation; 6-aminohexanenitrile; 1,6-hexanediamine.**

INTRODUCTION

Catalytic hydrogenation of nitriles is an important industrial route for the manufacture of a great variety of amines (1–3), especially of 1,6-hexanediamine and 6-aminohexanenitrile. This is confirmed by several recent patents (4–15). The hydrogenation of adiponitrile to 1,6-hexanediamine (16, 17) is an interesting industrial process in the preparation of Nylon-6,6 and also in the obtaining of 6-aminohexanenitrile (18, 19), which is used in the preparation of caprolactam (precursor of Nylon-6) (20).

Caprolactam is mainly produced from cyclohexanone, a process that generates 4.5 kg of ammonium sulfate per kg of caprolactam produced. However, Rhodia is developing a new salt-free process to obtain caprolactam at a lower cost than is needed for the current process. The first step of this new process is the hemihydrogenation of 1,6-hexanedinitrile (adiponitrile) to 6-aminohexanenitrile (21). This minimizes waste, one of the criteria of the green chemistry for the manufacture and application of chemical products (22).

[1] To whom correspondence should be addressed. Fax: +34 977559563. E-mail: salagre@quimica.urv.es.

The main products of nitrile hydrogenation are usually mixtures of amines (23, 24). The condensation reactions between a highly reactive intermediate imine and the primary amine always lead to the formation of products such as secondary and tertiary amines together with the primary amine (25). Catalysts based on Co, Ni, and Ru are mostly used to produce primary amines (6, 7, 13, 14, 18, 26–29).

The addition of potassium in small amounts enhances the selectivity of nickel catalysts toward primary amines in adiponitrile hydrogenation (30–33). Other precursors, such as hydrotalcites of Ni/Mg/Al, allow variation in the MgO/Al_2O_3 ratio and, thus, allow control of the acidity of the final catalysts (34, 35). When this ratio increases, the selectivity to primary amines increases for the hydrogenation of acetonitrile.

From studies of the preparation conditions of NiO–MgO systems, it is assumed that the reducibility of the corresponding NiO phase and the final properties of the nickel phase (size, morphology. . .) are highly affected by the tendency to form solid solutions of NiO–MgO (36–39). Additionally, Ni/MgO catalytic systems have shown to have a considerable inhibitory effect on the generation of graphitic residues in several reactions (40).

In previous work (41), Ni–MgO systems showed high activity for the hydrogenation of 1,4-butanedinitrile, with the highest selectivity, 85%, to 4-aminobutanenitrile. We also reported that the crystal morphology could induce certain selectivity to the monoamine (42–45). However, the recent literature on the hemihydrogenation of adiponitrile (4, 15, 17–19, 46–48) shows still difficulties in achieving selective hydrogenation with high conversion.

Our goal was to obtain nickel systems that can catalyze the hydrogenation of 1,6-hexanedinitrile and control the selectivity to 6-aminohexanenitrile and 1,6-hexanediamine. Therefore, two Ni–MgO catalysts were prepared and tested for the hydrogenation of adiponitrile. Their catalytic results are compared with those obtained for an usual industrial hydrogenation catalyst: Raney–Ni (7, 13).

0021-9517/02 $35.00

EXPERIMENTAL

Catalysts Preparation

Two NiO/MgO systems were prepared, with a weight ratio of 4 : 1 and a commercial MgO (Aldrich, 99%, BET area of 21 $m^2\ g^{-1}$) as the MgO source. Sample PA was prepared by thermal decomposition of a $Ni(NO_3)_2 \cdot 6H_2O$ and MgO mixture and subsequent calcination under static air according to a method previously described (41). Sample PB was prepared by means of controlled thermolysis of $Ni(NO_3)_2 \cdot 6H_2O$ at 373 K for 14 days to obtain $Ni_3(NO_3)_2(OH)_4$, which was then mixed with MgO. This mixture was subsequently calcined at 523 K under an argon flow.

The Raney–nickel was a commercial nickel sponge suspension in water (Fluka 99%) and was dried under H_2 flow at 453 K for 1 h (referred to as Raney–Ni). The NiO–MgO systems (PA and PB, catalysts A and B, respectively) were reduced under pure H_2 at 673 K for 6 h. The catalysts, after the catalytic reaction, were named Raney–Ni_{AC}, A_{AC}, and B_{AC}.

Characterization Methods

BET surface areas were calculated from the nitrogen adsorption isotherms at 77 K using a Micromeritics ASAP 2000 surface analyzer and a value of 0.164 nm^2 for the cross section of the nitrogen molecule.

Powder X-ray diffraction patterns of the samples were obtained with a Siemens D5000 diffractometer using nickel-filtered Cu $K\alpha$ radiation. This technique was also used to determine the reduction degree (α) of the catalysts by means of the Rietveld method (49). Temperature-programmed reduction studies (TPR) were carried out in a Labsys/Setaram TG DTA/DSC, equipped with a 273- to 1273-K programmable temperature furnace. Each sample was first heated at 423 K in an Ar flow until no change of weight was detected. Then, the sample was heated in a 5 vol% H_2/Ar flow from 423 to 1173 K at a rate of 5 K min^{-1}.

Hydrogen chemisorption was measured with a Micromeritics ASAP 2010C equipped with a turbomolecular pump. Samples had been previously reduced under the same conditions as for preparing the catalysts and the hydrogen was analyzed at 303 K. In chemisorption studies of nickel catalysts, Coenen pointed out the importance of employing a long equilibration time (50). A longer equilibration interval improves the data integrity and, consequently, higher chemisorption is obtained due to the slow equilibrium kinetics of hydrogen. In order to obtain the optimum amount of chemisorbed hydrogen for each catalyst, the equilibration intervals were increased until no different metallic area values were obtained. The nickel surface area was calculated assuming a stoichiometry of one hydrogen molecule per two surface nickel atoms and an atomic cross-sectional area of 6.49×10^{-20} m^2/Ni atom.

Temperature-programmed desorption (TPD) was obtained with a FISONS QTMD 150 gas desorption unit equipped with a 273- to 1273-K programmable temperature furnace and a mass spectrometer detector. Samples had been previously reduced under the same conditions as for preparing the catalysts. The desorption was carried out from room temperature to 1123 K at a rate of 10 K/min.

Scanning electron micrographs (SEM) were obtained with a JEOL JSM6400 scanning microscope operating at an accelerating voltage in the range 30–35 kV.

Determination of the Catalytic Activity

The gas-phase hydrogenation of 1,6-hexanedinitrile at atmospheric pressure (1 Torr) was studied in a tubular fixed-bed flow reactor heated by an oven equipped with a temperature control system. The reactor was filled with catalyst (500 mg of catalysts PA and PB and 314 mg of Raney–Ni). Reaction products were analyzed by an online gas chromatograph HP 5890 equipped with a 30-m "commercial Rtx-5 amine" cappillary column and a flame ionization detector.

RESULTS AND DISCUSSION

Characterization of the Catalyst Precursors

Table 1 shows characterization data of the catalyst precursors. Sample PA shows diffraction lines which can be identified as the NiO–MgO solid-solution phase (39, 41). In contrast, sample PB only has diffraction peaks of the NiO phase. The use of an argon flow through the sample during calcination could make the diffusion between the NiO and MgO phases for sample PB difficult. This is in agreement with Arena and co-workers, who reported the importance of diffusion on the formation of a solid solution (36, 37).

The reducibility of the two NiO–MgO systems was estimated by TPR by comparing their initial reduction temperature values (T_R). The initial reduction temperature of sample PB is considerably lower than that of sample PA (Table 1). This confirms the low interaction between the NiO and MgO phases for sample PB. The higher initial

TABLE 1

Characterization of the Catalytic Precursors

Catalytic precursors	PA	PB
Crystalline phases (XRD)	NiO–MgO	NiO
Crystallite sizes (nm)[a]	35.2	16.1
T_R (K) (TPR)[b]	604	523
Surface area ($m^2\ g^{-1}$)[c]	36.8	86.9

[a] Using Scherrer equation.

[b] T_R = initial reduction temperature, obtained by TPR experiments.

[c] Using BET area method.

reduction temperature of sample PA is in agreement with the results of Arena and co-workers, (36–38) and more-recent studies (39, 41), which reported that the formation of a solid solution hinders the reduction of NiO. Also, Ruckenstein and Hang Hu reported that the electronic transfer between NiO and MgO involves strong interactions, which inhibit the reduction of NiO (51). The surface area of the NiO–MgO systems is 36.8 $m^2\ g^{-1}$ for PA and 86.9 $m^2\ g^{-1}$ for PB (Table 1). The higher surface area of the catalytic precursor PB compared with that of PA could be due to the use of an argon flow. This favors the efficient elimination of decomposition products and, therefore, the agglomeration effect is lower.

The morphology and particle size for the different precursors of NiO–MgO has been observed by SEM. Samples PA and PB shows octahedral particles around 100–300 and 50–150 nm, respectively. The values observed are in agreement with the BET area results.

Characterization of the Catalysts before Reaction

Table 2 shows the crystalline phases obtained by XRD for the three catalysts and the reduction degree (α) at the given reduction conditions. The Raney–Ni and B catalysts have crystalline nickel as single phase and show total reduction ($\alpha = 1$). However, catalyst A shows a powder diffraction pattern corresponding to two phases: a crystalline solid-solution phase and a less crystalline Ni phase. The partial reduction obtained for catalyst A ($\alpha = 0.71$) is in agreement with the lower reducibility of its precursor, as observed by TPR.

After reduction, catalyst B exhibits a lower surface area (20.5 $m^2\ g^{-1}$) than its catalytic precursor (86.9 $m^2\ g^{-1}$). This decrease could be related to the fast reduction observed for this catalyst, which facilitates a higher agglomeration of metallic particles.

On the other hand, there are only slight differences in the BET area values for the precursor PA (36.8 $m^2\ g^{-1}$) and its corresponding catalyst A (42.3 $m^2\ g^{-1}$). This is in agreement with the better dispersion of NiO observed when the precursor is a solid solution. In that case, the reduction is slow and the sintering effect is smaller, as confirmed by its crystallite size (Table 2).

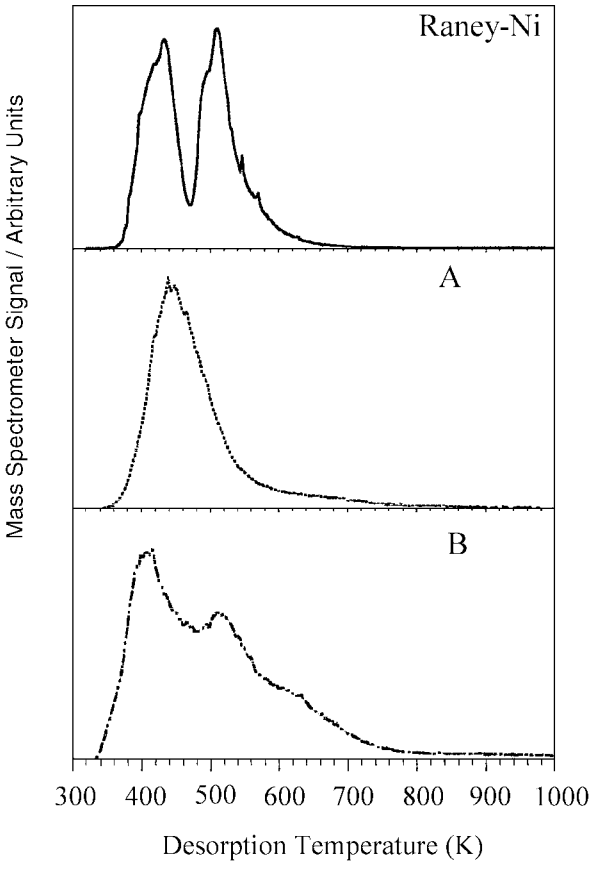

FIG. 1. H_2TPD plots for the three catalysts.

TABLE 2

Characterization of the Catalysts before Reaction

Catalysts	Raney–Ni	A	B
Crystalline phases (XRD)	Ni	Ni NiO–MgO	Ni
Crystallite sizes of Ni (nm)[a]	9.2	9.2	62.6
Surface area ($m^2\ g^{-1}$)[b]	72.8	42.3	20.5
Metallic area ($m^2\ g^{-1}$ catalyst)[c]	31.0	16.1	2.0
Reduction degree α[d]	1	0.71	1

[a] Using Scherrer equation.
[b] Using BET area method.
[c] Metal surface area, calculated from chemisorbed H_2.
[d] Reduction degree obtained by using the Rietveld method (49).

The surface area of the commercial Raney–Ni catalyst after drying at 453 K was high (72.8 $m^2\ g^{-1}$), as was expected from the sponge structure of this nickel.

Table 2 also shows the results of H_2 adsorption experiments. The Raney–Ni catalyst has a higher metallic area (31.0 $m^2\ g^{-1}$catalyst) than catalyst A (16.1 $m^2\ g^{-1}$catalyst) and catalyst B (2.0 $m^2\ g^{-1}$catalyst). These values are in agreement with their nickel crystallite sizes.

The difference between the two catalysts prepared with magnesia could be again related to a higher sintering effect produced during the reduction step for the sample that has not formed a solid solution. Therefore, catalyst B has a higher crystallite size and lower BET and metallic area values than does catalyst A.

The TPD hydrogen studies show some differences between the three catalysts. The Raney–Ni catalyst shows two hydrogen desorption peaks clearly differentiated, with similar intensity and with maxima at 427 and 505 K (Fig. 1). In contrast, catalyst A only shows one hydrogen desorption peak, with a maximum at 446 K, and catalyst B shows three maximum of hydrogen desorption, at 405, 513, and 606 K.

It is interesting that the TPD spectrum of catalyst B is similar to the TPD spectrum reported in a previous work for a bulk nickel catalyst, with octahedral crystals, which was obtained from decomposition of nickel nitrate (41). The difference is just a slight shift to lower temperatures for catalyst B. This catalyst also has a low metallic area as the bulk nickel catalyst. These similarities are probably related to the fact that catalyst B does not form a solid solution.

The SEM micrograph of catalyst A does not show significant differences in size and morphology with respect to its catalytic precursor. However, in the micrograph of catalyst B a partial agglomeration of particles was observed when compared with its catalytic precursor.

Characterization of the Catalysts after Catalytic Reaction

Table 3 shows the characterization of the catalysts after reaction. Catalysts A_{AC} and Raney–Ni_{AC} almost have the same nickel crystallite size (around 10 nm) as before catalysis. However, the surface areas (15.6 and 22.3 $m^2\ g^{-1}$) and metallic areas (2.5 and 4.2 $m^2\ g^{-1}$ catalyst) have decreased for both catalysts (A_{AC}, and Raney–Ni_{AC}, respectively). Finally, there is a slight decrease in metallic particle size (49.9 nm) together with a small increase in the surface area (26.5 $m^2\ g^{-1}$), but the metallic area decreases in slightly (1.6 $m^2\ g^{-1}$ catalyst) for catalyst B_{AC}.

The results obtained for catalysts A_{AC} and Raney–Ni_{AC} cannot be explained by the sintering of this nickel metallic phase because its crystallite size is maintained. The formation of small amounts of high-molecular-weight products at the reaction conditions tested can probably produce a partial coverage or decoration of the Ni particles, which could be responsible for the decrease in the surface area and metallic area. On the other hand, the surface modifications observed in catalyst B_{AC} could be related to two simultaneous effects: (i) a small disagglomeration of Ni and MgO particles during reaction, and (ii) a decoration, mainly of Ni particles, with the condensation products.

Figures 2a–2c show SEM micrographs of catalysts A_{AC}, B, and B_{AC}, respectively. After reaction, catalyst A shows similar sizes and octahedral morphologies as before reaction. However, for catalyst B, particles are better defined after reaction than before.

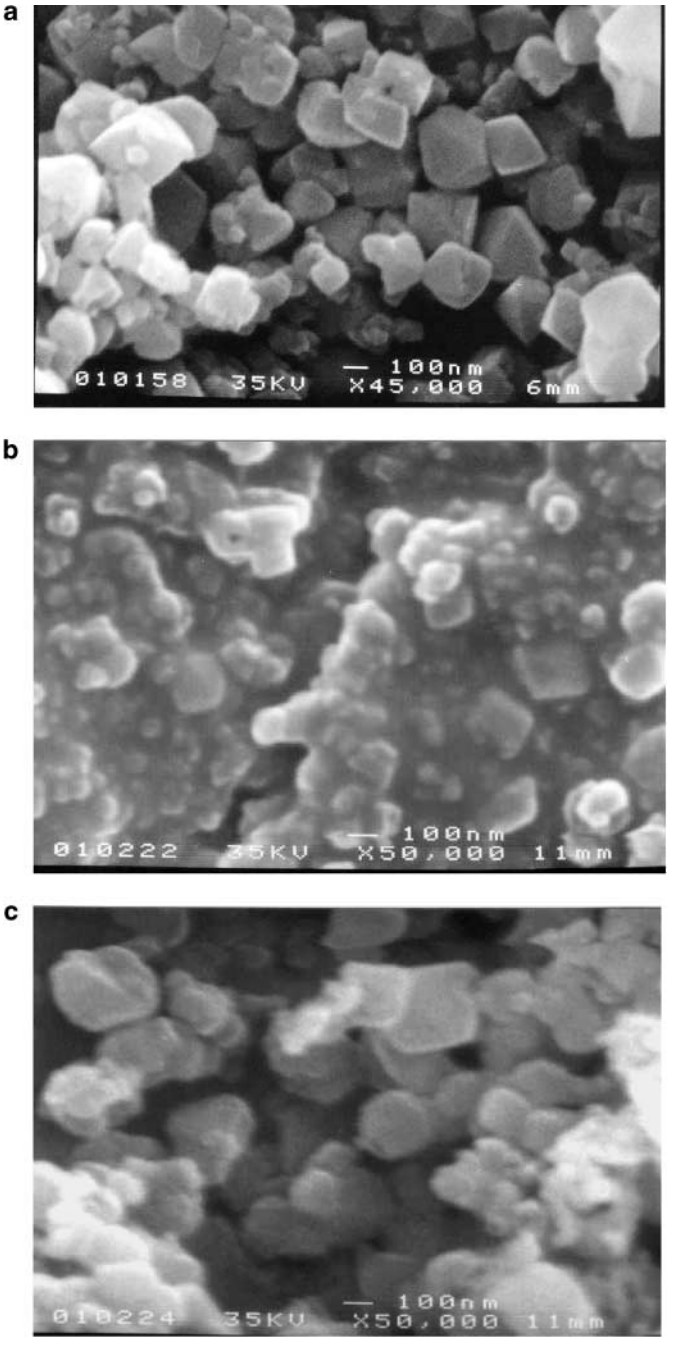

FIG. 2. Scanning electron micrographs of (a) catalyst A_{AC}, (b) catalyst B, and (c) catalyst B_{AC}.

TABLE 3

Characterization of the Catalysts after Reaction

Catalysts after reaction	Raney–Ni_{AC}	A_{AC}	B_{AC}
Crystalline phases (XRD)	Ni	Ni NiO–MgO	Ni
Crystallite sizes of Ni (nm)[a]	10.5	10.9	49.9
Surface area ($m^2\ g^{-1}$)[b]	22.3	15.6	26.5
Metallic area ($m^2\ g^{-1}$ catalyst)[c]	4.2	2.5	1.6

[a] Using Scherrer equation.
[b] Using BET area method.
[c] Metal surface area, calculated from chemisorbed H_2.

Catalytic Activity

Tables 4 and 5 show conversions and selectivities for the hydrogenation of 1,6-hexanedinitrile on nickel and nickel–magnesia catalysts (catalysts Raney–Ni, A, and B) under

TABLE 4

Catalytic Behavior of the Raney–Ni Catalyst for the Hydrogenation of 1,6-Hexanedinitrile

					Selectivity (%)					
Catalyst	H_2/ADN ratio	Space velocity (h^{-1})	Reaction temp. (K)	Conversion (%)	1-Azacyclo heptane (HHAPN)	3,4,5,6-Tetrahydro-2H-azepine (THAPN)	6-Aminohexane nitrile (AHN)	1,6-Hexane diamine (HMA)	Cracking products	Condensation products
Raney–Ni	6738	71,620	363	100	0	0	14	86	0	0
	1002	47,747	383	80	8	3	60	29	0	0
	1002	34,139	383	95	18	12	33	37	0	0
	178	23,873	423	100	45	0	0	36	11	8
	178	71,620	423	99	16	0	8	67	8	1
	59	71,620	423	64	14	4	33	32	15	2
	9	23,873	473	90	22	5	28	34	8	3
	9	5,968	473	100	53	0	0	17	25	5
	4	5,968	473	97	23	5	23	37	12	0

the conditions given under Experimental. The comparison of the catalytic activities of these catalysts was carried out at the same H_2/ADN ratios and using the same theoretical amount of Ni as for that of the active phase. Taking into account the fact that selectivity toward the different reaction products could be related to the reaction conditions (41), the comparative study was performed at different reaction temperatures, space velocities, and H_2/ADN molar ratios. In order to have the same H_2/ADN ratios for the three catalysts, the space velocities for the Raney–Ni catalyst were higher. The catalytic results for each catalyst are given in four groups of conditions: (a) ratio H_2/ADN = 6738, reaction temperature = 363 K; (b) H_2/ADN = 1002, reaction temperature = 383 K; (c) H_2/ADN = 178, reaction temperature = 423 K; and (d) H_2/ADN = 9, reaction temperature = 473 K. In addition, some results at lower H_2/ADN ratios at the same reaction temperature are also included for the Raney–Ni catalyst (Table 4).

By-products such as condensation compounds, which are dimers produced by an intermolecular amine–imine condensation reaction, were obtained in small amounts (0–9%) for all catalysts. For catalysts A and B, this is probably due to the basic character of magnesia, which favors the elimination of amines and prevents secondary reactions. These results are in agreement with those previously reported for the hydrogenation of 1,4-butanedinitrile (41). However, the Raney–Ni behavior could be related to its high activity, which favors the fast hydrogenation of the imine intermediate in front of the condensation reactions. Moreover, the Raney–Ni and A catalysts show the highest amount of

TABLE 5

Catalytic Behavior of Ni–MgO Catalysts for the Hydrogenation of 1,6-Hexanedinitrile

					Selectivity (%)					
Catalyst	H_2/ADN ratio	Space velocity (h^{-1})	Reaction temp. (K)	Conversion (%)	1-Azacyclo heptane (HHAPN)	3,4,5,6-Tetrahydro-2H-azepine (THAPN)	6-Aminohexane nitrile (AHN)	1,6-Hexane diamine (HMA)	Cracking products	Condensation products
A	6738	21,486	363	100	0	0	3	96	0	1
	1002	10,242	383	87	0	1	83	16	0	0
	178	1,790	423	100	60	0	0	28	5	7
	178	7,162	423	55	0	0	87	7	0	6
	9	895	473	93	44	2	1	5	48	0
	9	14,324	473	65	4	0	65	12	15	4
B	6738	21,486	363	100	12	0	1	84	0	0
	1002	10,242	383	85	23	0	77	0	0	0
	178	1,790	423	100	18	2	49	22	0	9
	178	7,162	423	30	2	2	81	8	1	6
	9	895	473	93	28	1	16	46	6	3
	9	14,324	473	56	3	1	77	15	1	3

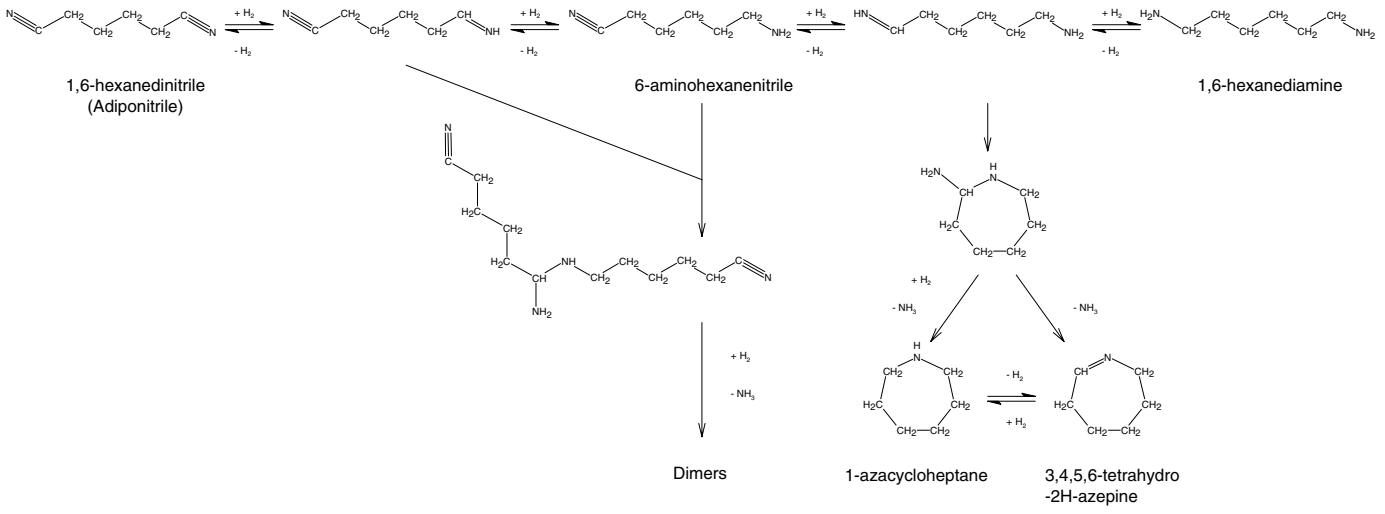

SCHEME 1. Possible products obtained by catalytic hydrogenation of 1,6-hexanedinitrile (adiponitrile).

cracking products (Tables 4 and 5), which can be related to their higher metallic areas.

The reaction mechanisms proposed in the literature for the hydrogenation of dinitriles show different reaction products of partial and total hydrogenation (23). This mechanism together with the results reported in recent studies for the hydrogenation of acetonitrile (52), 1,4-butanedinitrile (41), and 1,6-hexanedinitrile (42–45), and also with the results presented in this work, allows us to propose a sequence of the main catalytic hydrogenation products of 1,6-hexanedinitrile (Scheme 1).

This scheme shows that the formation of different products is directly related to the consumption of different amounts of hydrogen and to the hydrogenation rate of each step. Consequently, the selectivity could be controlled by means of the active hydrogen available (different for each catalyst and depending on the temperature reaction) and the contact time. The presence of cracking and cyclic products is probably related to more active systems (high hydrogen amounts available). The cyclic compound (HHAPN) needs the same theoretical hydrogen consumption as the diamine (HMA) but has a slower rate of formation and higher thermodynamic stability. Consequently, the production of HHAPN is favored at higher hydrogen amounts.

The results in Tables 4 and 5 show that the Raney–Ni catalyst is more active than the systems with magnesia at all reaction temperatures tested for the same H_2/ADN ratios (higher conversions, higher amounts of cyclic and cracking products at higher space velocities). At lower temperatures, the activity differences of Raney–Ni catalyst with the Ni–MgO catalysts decrease.

At reaction temperatures above 423 K, catalyst A is slightly more active than catalyst B (higher amounts of HHAPN). However, catalyst B seems slightly more active than catalyst A below 423 K (higher amounts of HHAPN). Actually, taking into account the metallic area and TPD results, small differences could be expected. There are great differences in the metallic area values between the three catalysts before reaction, but, after reaction, these differences decrease considerably (Tables 2 and 3).

Some authors correlated the binding strength of the chemisorbed hydrogen with the activity for a specific reaction (53–56). In our experiments the activity for each catalyst could be related to its hydrogen TPD values. Catalyst B has the lowest metallic area but its hydrogen desorption starts before that of the other catalysts (405 K). This could explain its higher activity at lower temperatures. The higher activity observed for catalyst A at higher reaction temperatures could also be explained by its metallic area and its maximum hydrogen desorption at 446 K.

Formation of 1,6-Hexanediamine

All catalysts show high selectivity toward 1,6-hexanediamine, with values of 86% for the Raney–Ni catalyst and 84% for catalyst B as total conversion. Catalyst A shows the highest selectivity to 1,6-hexanediamine (96%) also as total conversion and at the same reaction conditions (363 K and H_2/ADN = 6738) as the other catalysts.

In Scheme 1 we can see that cyclization products can compete with diamine when the hydrogen amount increases. However, in Tables 4 and 5 we observe that at lower temperature and higher space velocity, the diamine formation is favored. This is in agreement with results reported previously (41).

The small differences observed between the three catalysts could be related to similar amounts of hydrogen available at lower temperature (Fig. 1). The second product obtained was 1-azacycloheptane (12%) for catalyst B. However, catalyst A has only one hydrogen desorption peak (maximum at 446 K), an amount insufficient to produce the slow cyclization reaction at lower reaction

temperatures, and therefore, 1-azacycloheptane is not observed. The higher space velocity used for Raney–Ni (71,620 h^{-1}) than for the others (21,486 h^{-1}) explains the formation of 6-aminohexanenitrile (14%) for this catalyst.

We can conclude that the formation of 1,6-hexanedi amine with these nickel catalysts is favored at high H_2/ADN ratios and at lower reaction temperatures since higher reaction temperatures lead to cyclization (1-azacycloheptane) and cracking products.

Formation of 6-Aminohexanenitrile

Scheme 1 shows that the production of 6-aminohexanenitrile demands the lowest hydrogen consumption. In a previous work about the catalytic hydrogenation of 1,4-butanedinitrile with nickel–magnesia catalysts (41), we reported that when using low reaction temperatures, the amount of hydrogen available for these catalysts decreases, and consequently, the formation of the less hydrogenated species (4-aminobutanenitrile) increases. However, there are other parameters that influence the hydrogen consumption (ADN amounts, hydrogen flow, and contact time).

In order to obtain high activity and selectivity to monoamine at different reaction temperatures, three different strategies have been proposed:

(a) A reaction temperature at 383 K, low ADN vapor pressure (0.38 Torr), medium values of the H_2/ADN ratio (1002), and a space velocity of 10,242 h^{-1} have been used. In addition, higher space velocities have been used (47,747 and 34,139 h^{-1}) for Raney–Ni catalyst.

A low vapor pressure gives rise to small amounts of adiponitrile passing through the reactor. This, together with the reaction parameters, leads to higher conversions (between 80 and 95%) for all catalysts. Catalysts A and B show high selectivities to 6-aminohexanenitrile (83 and 77%). In contrast, the best result for the Raney–Ni catalyst is slightly lower, 60% of monamine for 80% of conversion at the higher space velocity of 47,747 h^{-1}. When decreasing the space velocity (34,139 h^{-1}) the conversion increases (up to 95%) but the selectivity to 6-aminohexanenitrile decreases to 33%, as expected.

(b) A reaction temperature at 423 K, moderate vapor pressure (4.28 Torr), and moderate H_2/ADN ratios (178) have also been used. These conditions allow a considerable decrease in the hydrogen amount needed. However, an increase in the contact time was necessary to not decrease the conversion for catalysts A and B too much (space velocity of 7162 h^{-1}). For the Raney–Ni catalysts, higher space velocities were tested (23,873 and 71,620 h^{-1}).

Again, catalysts A and B present a high selectivity to monoamine (87 and 81%, respectively). However, their conversions are lower (55 and 30%, respectively) than when using strategy (a). The Raney–Ni catalyst has very low selectivity to monoamine (8% at 71,620 h^{-1} and 0% at 23,873 h^{-1}) for a total conversion.

In order to improve the monoamine selectivity for the Raney–Ni catalyst, another reaction condition was tested: a lower ratio H_2/ADN (59) at the highest space velocity (71,620 h^{-1}). There was a slight increase in the selectivity to 6-aminohexanenitrile (33%) but the conversion was lower (64%).

(c) A reaction temperature at 473 K, high vapor pressure (98.6 Torr) of adiponitrile, low H_2/ADN ratio (9), and a space velocity of 14,324 h^{-1} for catalysts A and B have been used. Under these conditions, the small hydrogen amount and the low contact time of adiponitrile in the reactor counteract the effect of the high reaction temperature. For the Raney–Ni catalyst, a higher space velocity was tested (23,873 h^{-1}).

Catalysts A and B show high selectivity to monoamine (65 and 77%, respectively). However, the conversions are lower than when using strategy (a) (65 and 56%, respectively). Also, under these conditions, the Raney–Ni catalyst shows a lower selectivity to monoamine (28%) for a 90% conversion.

In order to obtain more information about the catalytic behavior of Raney–Ni, other reaction conditions were tested: space velocity of 5968 h^{-1} for 9 and 4 H_2/ADN ratios. Now, by decreasing the H_2/ADN ratio, the selectivity to monoamine increases from 0 to 23% for a similar conversion.

Independently of the reaction conditions used, the catalysts with magnesia presented high selectivities to 6-aminohexanenitrile. However, not all the strategies designed for Raney–Ni catalyst allowed a high selectivity to the monoamine to be obtained.

From these results, we can assume that the reaction conditions play an important role in controlling the selectivity for the hydrogenation of 1,6-hexanedinitrile. In addition, the difference observed between the Ni–MgO and Raney–Ni catalysts could also be explained by taking into account the effect of the particle morphology on selectivity to 6-aminohexanenitrile. In previous studies (41, 42–45), we reported that octahedral crystal sites could induce a certain selectivity to monoamine compounds. The results presented in this work support this approach since catalysts A and B, which present the higher selectivity to 6-aminohexanenitrile, show a considerable number of octahedral crystallites.

CONCLUSIONS

Two different nickel–magnesia catalysts were prepared by two different paths and compared with a commercial Raney–Ni catalyst for the hydrogenation of 1,6-hexanedinitrile (adiponitrile).

All catalysts showed high selectivity to 1,6-hexanediamine, for a total conversion at 363 K with a maximum of 96% for catalyst A, which is the Ni–MgO catalyst which

has a solid-solution phase. This similar behavior can be related to the similar amounts of hydrogen available at lower reaction temperatures for the three catalysts.

The Ni–MgO catalysts A and B showed a higher selectivity to the 6-aminohexanenitrile than did Raney–Ni at all conditions tested. It is possible to obtain high selectivity to the monoamine at different reaction conditions for catalysts A and B. A decrease in some reaction parameters (reaction temperature, H_2/ADN ratio, and contact time) favors the partial hydrogenation. Catalysts A and B showed the highest selectivity to 6-aminohexanenitrile (83 and 77%, respectively) with higher conversions (87 and 85%, respectively) at 383 K, a H_2/ADN ratio of 1002, and a space velocity of 10,242 h^{-1}. The high selectivity to 6-aminohexanenitrile could also be related to the presence of octahedral crystallites, which could induce selectivity to monoamine for catalyst A and B.

These preliminary studies make as believe that these Ni–MgO catalysts are suitable for the industrial manufacture of 1,6-hexanediamine and 6-aminohexanenitrile with high selectivity and conversion. However, information about lifetimes at the different reaction conditions is needed.

REFERENCES

1. Weissermel, K., and Arpe, H. J., "Industrial Organic Chemistry." Verlag Chemie, Berlin, 1978.
2. Volf, J., and Pasek, J., *Stud. Surf. Sci. Catal*. **27**, 105 (1986).
3. Prins, R., *Catal. Today* **37**, 103 (1997).
4. Vandenbooren, F., Bosman, H., and Van der Spoel, J., WIPO Patent WO9426699 A1 (1994) (DSM N.V.).
5. Cordier, G., Fouilloux, P., Laurain, N., and Spindler, J. F., WIPO Patent WO9518090 A1 (1995) (Rhone Poulenc Chimie).
6. Schnurr, W., Voit, G., Flick, K., Melder, J. P., Fischer, R., and Harder, W., WIPO Patent WO9737964 A1 (1997) (BASF AKTIENGESELLSCHAFT).
7. Koch, T. A., Krause, K. R., and Sengupta, S. K., WIPO Patent WO9843940A1 (1998) (E. I. DuPont de Nemours and Co.).
8. Leconte, P., WIPO Patent WO9959962A1 (1998) (Rhodia Fiber and Resin Intermediates).
9. Boschat, V., Leconte, P., Rochette, D., and Sever, L., WIPO Patent WO9926917A1 (1999) (Rhodia Fiber and Resin Intermediates).
10. Luyken, H., Ohbach, F., Ansmann, A., Bassler, P., Fischer, R., Melder, J. P., Merger, M., Rehfinger, A., Voit, G., and Achhammer, G., WIPO Patent WO005191A1 (2000) (BASF AKTIENGESELLSCHAFT).
11. Luyken, H., Ohbach, F., Ansmann, A., Bassler, P., Fischer, R., Melder, J. P., Merger, M., Rehfinger, A., Voit, G., and Achhammer, G., WIPO Patent WO012459A1 (2000) (BASF AKTIENGESELLSCHAFT).
12. Fischer, R., Bassler, P., Luyken, H., Ohbach, F., Melder, J. P., Merger, M., Ansmann, A., Rehfinger, A., and Voit, G., WIPO Patent WO012460A1 (2000) (BASF AKTIENGESELLSCHAFT).
13. Boschat, V., and Brunelle, J. P., WIPO Patent WO027806A1 (2000) (Rhodia Fiber and Resin Intermediates).
14. Harper, M. J., WIPO Patent WO027526A1 (2000) (E. I. DuPont de Nemours and Co.).
15. Ionkin, A. S., Ziemecki, S. B., Koch, T. A., and Bryndza, H. E., WIPO Patent WO064862A3 (2000).
16. Lazaris, A. Y., Zilberman, E. N., Lunicheva, E. V., and Vedin, A. M., *Zh. Prikl. Khim.* **38**, 1097 (1965).
17. Medina, F., Salagre, P., Sueiras, J. E., and Fierro, J. L. G., *J. Mol. Catal.* **68**, L17 (1991).
18. Diamond, S. E., Mares F., and Szalkiewicz, A., EPO Patent EP077911A1 (1983) (Allied Corp.).
19. Sanchez, K. M., EPO Patent EP642493B1 (1996) (E. I. DuPont Nemours and Co.).
20. Brunelle, J. P., Seigneurin, A., and Sever, L., WIPO Patent WO005203A1 (2000) (Rhodia Fiber and Resin Intermediates).
21. Sheldon, R., *Green Chem.* **2**(1), G1 (2000).
22. Clark, J., *Green Chem.* **1**(1), 1 (2000).
23. Mares, F., Galle, J. E., Diamond, S. E., and Regina, F. J., *J. Catal.* **112**, 145 (1988).
24. Huang, Y., and Sachtler, W. M. H., *Appl. Catal. A* **182**, 365 (1999).
25. Augustine, R. L., *Catal. Rev.* **13**, 285 (1976).
26. Frank, G., and Neubauer, G., Germany Patent DE3402734A1 (1984) (BASF AKTIENGESELLSCHAFT).
27. Greenfield, H., *Ind. Eng. Chem. Prod. Res. Dev.* **6**, 142 (1967).
28. Pasek, J., Kostova, N., and Dvorak, B., *Collect. Czech. Chem. Commun.* **46**, 1011 (1981).
29. Schowoegler, E. J., and Adkins, H., *J. Am. Chem. Soc.* **61**, 3449 (1939).
30. Medina, F., Salagre, P., Sueiras, J. E., and Fierro, J. L. G., *Appl. Catal. A* **92**, 131 (1992).
31. Medina, F., Salagre, P., Sueiras, J. E., and Fierro, J. L. G., *Solid State Ionics* **59**, 205 (1993).
32. Medina, F., Salagre, P., Sueiras, J. E., and Fierro, J. L. G., *Appl. Catal. A* **99**, 115 (1993).
33. Medina, F., Salagre, P., Sueiras, J. E., and Fierro, J. L. G., *J. Chem. Soc. Faraday Trans.* **90**(10), 1455 (1994).
34. Medina, F., Dutartre, R., Tichit, D., Coq, B., Dung, N. T., Salagre, P., and Sueiras, J. E., *J. Mol. Catal. A* **119**, 201 (1997).
35. Dung, N. T., Tichit, D., Chiche, B. H., and Coq, B., *Appl. Catal. A* **169**, 179 (1998).
36. Parmaliana, A., Arena, F., Frusteri, F., and Giordano, N., *J. Chem. Soc. Faraday Trans.* **86**(14), 2663 (1990).
37. Arena, F., Frusteri, F., Parmaliana, A., Plyasova, L., and Shmakov, A. N., *J. Chem. Soc. Faraday Trans.* **92**, 469 (1996).
38. Arena, F., Frusteri, F., and Parmaliana, A., *Appl. Catal. A* **187**, 127 (1999).
39. Serra, M., Salagre, P., Cesteros, Y., Medina, F., and Sueiras, J. E., *Solid State Ionics* **134**, 229 (2000).
40. Bhattacharyya, A., and Chang, W. W., *Stud. Surf. Sci. Catal.* **88**, 207 (1994).
41. Serra, M., Salagre, P., Cesteros, Y., Medina, F., and Sueiras, J. E., *J. Catal.* **197**, 210 (2001).
42. Medina, F., Salagre, P., Sueiras, J. E., and Fierro, J. L. G., *J. Catal.* **142**, 392 (1993).
43. Medina, F., Salagre, P., Sueiras, J. E., and Fierro, J. L. G., *J. Mol. Catal.* **81**, 363 (1993).
44. Medina, F., Salagre, P., Sueiras, J. E., and Fierro, J. L. G., *J. Chem. Soc. Faraday Trans.* **89**(18), 3507 (1993).
45. Medina, F., Salagre, P., Sueiras, J. E., and Fierro, J. L. G., *J. Chem. Soc. Faraday Trans.* **89**(21), 3981 (1993).
46. Yu, X., Li, H., and Deng, J. F., *Appl. Catal. A* **199**, 191 (2000).
47. Li, H., Xu, Y., Li, H., and Deng, J. F., *Appl. Catal. A* **216**, 51 (2001).
48. Li, H., Xu, Y., and Deng, J. F., *New J. Chem.* **11**, 1059 (1999).
49. Bish, D. L., and Howard, S. A., *J. Appl. Cryst.* **21**, 86 (1988).
50. Coenen, J. W. E., *Appl. Catal.* **75**, 193 (1991).
51. Ruckenstein, E., and Hang Hu, Y., *Appl. Catal. A* **183**, 85 (1999).
52. Verhaak, M. J. F. M., Van Dillen, A. J., and Geus, J. W., *J. Catal.* **143**, 187 (1993).
53. Smeds, S., Salmi, T., Lindfors, L. P., and Krause, O., *Appl. Catal. A* **144**, 177 (1996).
54. Cesteros, Y., Salagre, P., Medina, F., and Sueiras, J. E., *Appl. Catal. B* **25**, 213 (2000).
55. Cesteros, Y., Salagre, P., Medina, F., and Sueiras, J. E., *Appl. Catal. B* **22**, 135 (1999).
56. Marécot, P., Paraiso, E., Dumas, J. M., and Barbier, J., *Appl. Catal.* **74**, 261 (1991).